sustainability

MDPI

Article

Multi-Scale Minero-Chemical Analysis of Biomass Ashes: A Key to Evaluating Their Dangers vs. Benefits

Paola Comodi [1,*], Azzurra Zucchini [1], Umberto Susta [2], Costanza Cambi [1], Riccardo Vivani [3], Gianluca Cavalaglio [4] and Franco Cotana [5]

1 Dipartimento di Fisica e Geologia, Università degli Studi di Perugia, 06121 Perugia, Italy; azzurra.zucchini@unipg.it (A.Z.); costanza.cambi@unipg.it (C.C.)
2 UOC PSAL, AUSL Umbria 1, 06127 Perugia, Italy; umberto.susta@uslumbria1.it
3 Dipartimento di Scienze Farmaceutiche, Università degli Studi di Perugia, 06121 Perugia, Italy; riccardo.vivani@unipg.it
4 Dipartimento di Giurisprudenza, Università Telematica Pegaso, 80132 Napoli, Italy; gianluca.cavalaglio@unipegaso.it
5 Dipartimento di Ingegneria, Università degli Studi di Perugia, 06121 Perugia, Italy; franco.cotana@unipg.it
* Correspondence: paola.comodi@unipg.it

Abstract: A multi-methodic analysis was performed on five samples of fly ashes coming from different biomasses. The aim of the study was to evaluate their possible re-use and their dangerousness to people and the environment. Optical granulometric analyses indicated that the average diameter of the studied fly ashes was around 20 μm, whereas only ~1 vol% had diameters lower that 2.5 μm. The chemical composition, investigated with electron probe microanalysis, indicated that all the samples had a composition in which Ca was prevalent, followed by Si and Al. Large contents of K and P were observed in some samples, whereas the amount of potentially toxic elements was always below the Italian law thresholds. Polycyclic aromatic hydrocarbons were completely absent in all the samples coming from combustion plants, whereas they were present in the fly ashes from the gasification center. Quantitative mineralogical content, determined by Rietveld analysis of X-ray powder diffraction data, indicated that all the samples had high amorphous content, likely enriched in Ca, and several K and P minerals, such as sylvite and apatite. The results obtained from the chemo-mineralogical study performed make it possible to point out that biomass fly ashes could be interesting materials (1) for amendments in clayey soils, as a substitution for lime, to stimulate pozzolanic reactions and improve their geotechnical properties, thus, on the one hand, avoiding the need to mine raw materials and, on the other hand, re-cycling waste; and (2) as agricultural fertilizers made by a new and ecological source of K and P.

Keywords: biomass; fly ashes; X-ray diffraction; chemical analysis; multi-methodic analysis

Citation: Comodi, P.; Zucchini, A.; Susta, U.; Cambi, C.; Vivani, R.; Cavalaglio, G.; Cotana, F. Multi-Scale Minero-Chemical Analysis of Biomass Ashes: A Key to Evaluating Their Dangers vs. Benefits. *Sustainability* **2021**, *13*, 6052. https://doi.org/10.3390/su13116052

Academic Editors: Petronela Nechita, Rodica-Mihaela Dinică and Bianca Furdui

Received: 7 May 2021
Accepted: 25 May 2021
Published: 27 May 2021
Corrected: 16 November 2021

1. Introduction

Fly ashes represent the amount of solid, inorganic residue left after the complete burning of biomasses. They are an integral part of plant materials and can have a wide range of elements. Due to the difference in raw materials as well as in the combustion plant type, the chemical physical characteristics of fly ashes can be quite different [1]. Moreover, the percentage of ashes produced during biomass burning varies according to the biomass type, ranging from a few units to about 10 dry weight percent [2,3].

Several papers [4–6] have shown that the principal chemical components of biomass ashes are silicon, aluminum, calcium, iron, magnesium, and sodium, together with valuable amounts of important plant nutrients, such as potassium and phosphorous.

The strong push towards the reuse of materials, together with the likely large increase of fly ashes from biomass over the last decades, suggest the need to take actions devoted to their re-use as second generation products [7]. Important examples include in

agriculture, where biomass fly ashes are used either as fertilizers or as raw materials to manufacture fertilizers, and in the concrete industry, where biomass fly ashes are used as an aggregate/binder in concrete production (see [8] and references therein), contributing to enhancing the sustainability of the concrete industry. In particular, biomass ashes, e.g., from sugarcane bagasse, forest residues, or wheat straw, can be added to concrete as relevant components due to their pozzolanic properties [9–12].

On the other hand, they also can be used for producing silicon-based materials because of their very high silica content or in soil stabilization management [13,14].

Due to their broad range of features, the identification of beneficial re-uses must pass through the detailed characterization of biomass fly ashes. The chemical composition of biomass ashes is usually represented by the macro-elements Ca, K, P, and S, which suggest the possibility of their agricultural use [15], but they can contain heavy metals [16], as well as polycyclic aromatic hydrocarbons (PAHs) that can be produced by the thermal decomposition of organic matter due to incomplete combustion, e.g., either in engines and incinerators or when biomass burns in forest fires. Domestic wood burning and road traffic are the major sources of PAHs [17].

These components can hinder the use of biomass ashes due to their the cancerogenic character [18] and thus they should be monitored before being reused in a sustainable way, either directly as fertilizers or as raw material to manufacture fertilizers, and returned to soils.

Cabrera et al. [11] have characterized the biomass performances (energetic, physical, and chemical) of different biomass feedstocks, including lignocellulosic residues of cardoon energy crops, residues from the pruning of grapevines and olive trees, and residues from river maintenance (turkey oak). Each biomass sample was characterized in terms of the moisture content, ashes content, volatile substances, fixed carbon, low and high heating values [19], and the content levels of carbon, nitrogen, hydrogen, and the main metals [20]

This study aimed to investigate, with a multi-methodic approach, a group of ash products from different biomasses and from different combustion plants. Some of these samples have already been characterized in [3] and this allowed us to relate the characteristics of raw materials with those of ashes. In addition, a sample from a gasification plant and a sample from pellet combustions were investigated.

The samples were characterized from morphological, chemical, and mineralogical points of view. In particular, granulometric analysis was performed by diffraction light scattering and optical analysis in order to determine the PM10 and PM2.5 fractions which could impact on air pollution. X-ray powder diffraction (XRPD) analysis was used to determine the amount of the amorphous component, as well the crystalline fraction, in order to define the forms in which the chemical component are allocated and their availability and solubility for agricultural and/or other employments [21]. Thermal analyses (TA) were used to investigate the loss of mass during heating cycles and to determine the amount of volatile components. Moreover, bulk chemical analysis of major, minor, and trace elements (in particular heavy metals and potentially toxic elements (PTEs)) were deployed by means of an electron microprobe coupled with the wavelength dispersive spectroscopy (EMPA-WDS) technique. Field emission scanning electron microscopy (FE-SEM), coupled with microanalysis (energy dispersive spectroscopy (EDS)), was used to investigate micro-textural characteristics, especially focusing on the analysis of the possible occurrence of either concentric or zoned element distributions. Lastly, gas chromatography was used to determine PAH contents.

2. Materials and Methods

2.1. Samples

The type and the origin of samples investigated in this study are reported in Table 1.

Table 1. Samples used in the present work.

Code	Name/Type	Origin
#1	Sample 1 biomass ashes	Gasification power plant, Magione (PG), Italy
#2	Sample 2 biomass ashes	Grapevine prunings, Torgiano (PG), Italy
#3	Sample 3 biomass ashes	Wood pellets
#4	Sample 4 biomass ashes	Olive tree prunings
#5	Sample 5 biomass ashes	Cardoon plants

2.2. Experimental Thecniques

2.2.1. XRPD Analyses

X-ray powder diffraction analyses were performed on randomly oriented powder at room temperature using a Phillips PW-1830, equipped with a graphite monochromator on the outgoing rays, and using CuK_α radiation (λ = 1.5406). The voltage and current intensity of the generator were 40 kV and 30 mA, the step size was 0.3°, and the acquisition time for each step was 18 s. The diffraction patterns were collected in a Bragg–Brentano geometry (θ–2θ), in a range of 2θ between 5° to 80°. The Rietveld method [22], as implemented in GSAS—EXPGUI [23,24], was used for quantitative mineralogical analysis of the samples. A fraction of 10% by weight of crystalline silicon (Si) was added as external standard for the determination of the amorphous content. The background was fitted with a Chebyshev polynomial function and diffraction peaks were modeled with a pseudo-Voight function. Scale factor, lattice constants, and coefficients for the peak shapes were refined for each phase.

2.2.2. TGA and DTA

Thermogravimetric analyses (TGAs) were performed with a Netzsch STA 449F3. Approximately 50 to 100 mg of finely ground material was heated at a rate of 10 °C min^{-1}, under room atmosphere, from 20 °C up to 1000 °C. The Netzsch software was used to process the results at the Department of Chemistry of Perugia University, Italy.

Differential thermal analysis (DTA) is a thermal analysis technique in which the heat flow into or out of a sample is measured as a function of temperature or time while the sample is exposed to a controlled temperature program. It is a very powerful technique for the evaluation of material properties such as glass transition temperature, melting temperature, crystallization, specific heat capacity, cure process, purity, oxidation behavior, and thermal stability.

2.2.3. SEM Analyses

The surface morphology and the chemical composition were examined through field emission scanning electron microscopy (FE-SEM) using an LEO 1525 with a ZEISS AsB (angle-selective backscatter) detector (Oberkochen, Germany), available at the Department of Physics and Geology of the University of Perugia. The FE-SEM instrument was coupled with EDS microanalysis (BrukerQuantax EDS). Gold coating was applied for SEM observations.

2.2.4. Granulometric Analysis

Particle sizes greater than 3 microns were determined by using an Accusizer TM Optical Particle Sizer Model 770 (Santa Barbara, CA, USA), whereas, for particle sizes lower than 3 microns, the dynamic light scattering technique was employed by using a NICOMP 380 ZLS zeta potential/particle sizer (PSS NICOMP; Santa Barbara, CA, USA). Approximately 10 mg of each sample was dispersed in 1 mL of bi-distilled water and sonicated for 10 s to improve the dispersion of the single particles.

2.2.5. EMPA and LA-ICP-MS Analyses

The samples were also analyzed in terms of bulk composition. In order to obtain homogeneous pellets, the ashes were heat-treated up to and beyond their fusion points.

The heating was performed by putting a few grams of each specimen into a crucible made out of pure Pt and using a muffle capable of heating to 1600 °C. Once the samples were completely molten, they were quickly quenched at room temperature. The glass pellets obtained after the quenching were embedded with epoxy resin; the mounts were cut, ground, and highly polished down to a 1 µm grade diamond polishing paste. Minor and trace elements were analysed at the Department of Physics and Geology (Perugia University) by LA-ICP-MS using the analytical protocol reported in Ref. [25].

Before being analyzed, each polished mount had to be coated using graphite. EMPA–WDS analyses were carried out at the Electron Microprobe Laboratory of the Earth Science Department "Ardito Desio" (University of Milan, Milan, Italy), using the EMPA–WDS JEOL 8200 Super Probe with 5 WDS channels and one EDS channel under the following operating conditions: accelerating voltage, 15 kV; beam current, 5 nA; counting time, 30 s for all the elements and 10 s for the backgrounds. Calibration for chemical analysis was accomplished with a set of synthetic and natural standards, including: grossular (Al, Si, Ca), omphacite (Na), olivine (Mg), apatite (P), scapolite (Cl), pure Cr, rhodonite (Mn), fayalite (Fe), K-feldspar (K), and ilmenite (Ti).

2.2.6. PAHs (Polycyclic Aromatic Hydrocarbons)

To evaluate the possibly dangerous character of fly ashes and to determine their possible employments, polycyclic aromatic hydrocarbons measurements were performed.

The samples were analyzed with gas chromatography (Agilent mod. 6890) coupled with mass spectrometry (5973N, Agilent Technologies), using reference standards.

The total amounts of PAHs, including naftalene, acenaftene, acenaftilene, fluorene, fenatrene, antracene, fluoratene, pirene, benzoantracene crysene, benzo(b,k,j) fluorantene, benzo(e)pirene, benzo(a)pirene, indenopirene, dibenzo(a,h)antracene, and benzo(g,h,i)perilene, were determined.

3. Results

3.1. Granulometric Results

The results of the granulometric analysis are reported in Figure 1. The average sizes were quite similar for the five samples and equal to 23.8, 17.0, 21.0, 21.0, and 18 µm, from sample 1 to 5.

On the other hand, more relevant differences can be seen from the analysis of the granulometric curves reported in Figure 1, where the red lines highlight the positions of the 2.5 and 10 µm diameter particles. These values represent important limits as they identify the inhalation properties and, thus, the health hazard with regard to their inhalation capacities.

All samples contained very low percentages of particles with dimensions under 2.5 µm (less than 1 vol%), whereas the contents in particles with diameters less than 10 µm was quite different, varying from 5 vol% in sample 5 to 40 vol% in sample 4.

3.2. X-ray Diffraction Results

The quantitative mineralogical composition, as well as the amount of amorphous components, are reported in Table 2, whereas Figure 2 shows the X-ray diffraction profiles collected and calculated with Rietveld analyses. In particular, in the graphs, the red crosses represent the data collected and the green lines represent the calculated best-fitting profiles, obtained by adding in the refinements of the minerals reported in Table 2. The theoretical peak positions of each mineral are reported under the profile, i.e., each horizontal line with different bars represents the theoretical peak position for that mineral. The lowest bar line reports the theoretical peak position of metallic Si, added to each sample as an internal standard for the quantitative analysis. The pink profile in the lower part of each graph represents the difference profile generated by subtracting the measured profile from the calculated one [24].

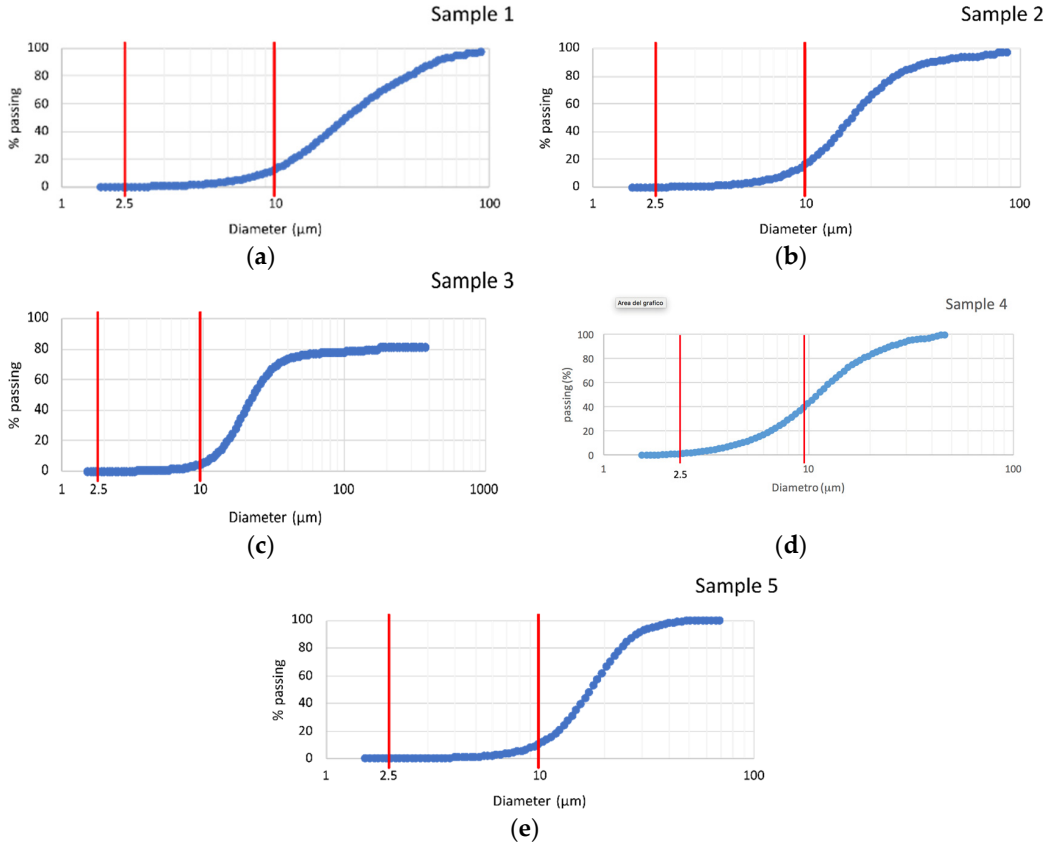

Figure 1. Average grain size distribution for the five samples determined by dynamic light scattering. Samples from 1 to 5 are shown from (**a**–**e**). The vertical red lines highlight the 10 and 2.5 micron diameters.

Table 2. Quantitative analysis by Rietveld refinement of XRPD data. Quantitative results are given in wt%. Errors in wt% are also listed. Amorphous content was recalculated based on Si as an external standard.

Sample	Phases	Chemical Formula	wt%	Error
#1	Quartz	SiO_2	2.91	0.01
	Calcite	$CaCO_3$	21.01	0.07
	Portlandite	$CaO(OH)_2$	4.47	0.05
	Sulphur	S	0.41	0.02
	Hydroxylapatite	$Ca_5(PO_4)_3(OH)$	3.11	0.02
	Amorphous		68.1	0.1
#2	Periclase	MgO	1.81	0.01
	Calcite	$CaCO_3$	8.34	0.04
	Heulandite	$(Ca.Na)_{2–3}Al_3(Al.Si)_2Si_{13}O_{36}·12(H_2O)$	1.15	0.03
	Calcioferrite	$Ca_4Fe^{2+}(Fe^{3+}.Al)_4(PO_4)_6(OH)_4·12(H_2O)$	1.60	0.02
	Fairchildite	$K_2Ca(CO_3)_2$	2.23	0.01
	Quartz	SiO_2	0.33	0.11
	Hydroxylapatite	$Ca_5(PO_4)_3(OH)$	5.08	0.21
	Amorphous		79.5	0.2
#3	Periclase	MgO	5.77	0.02
	Calcite	$CaCO_3$	6.36	0.05
	Portlandite	$Ca(OH)_2$	0.63	0.04
	Lime	CaO	2.06	0.02
	Fairchildite	$K_2Ca(CO_3)_2$	11.20	0.03
	Quartz	SiO_2	0.52	0.14
	Apatite	$Ca_5(PO_4)_3(OH.F.Cl)$	1.39	0.26
	Amorphous		72.1	0.3

Table 2. *Cont.*

Sample	Phases	Chemical Formula	wt%	Error
#4	Reichenbachite	$Cu^{2+}{}_5(PO_4)_2(OH)_4$	0.95	0.02
	Calcite	$CaCO_3$	42.24	0.15
	Quartz	SiO_2	4.18	0.07
	Phosphoferrite	$(Fe^{2+}.Mn)_3(PO_4)_2{\cdot}3(H_2O)$	0.42	0.03
	Hydrossilapatite	$Ca_5(PO_4)_3(OH)$	4.57	0.03
	Amorphous		47.6	0.5
#5	Lime	CaO	0.08	0.01
	Calcite	$CaCO_3$	6.62	0.03
	Fluellite	$Al_2(PO_4)F_2(OH){\cdot}7(H_2O)$	3.48	0.03
	Sylvite	KCl	2.99	0.01
	Quartz	SiO_2	0.28	0.01
	Rhodochrosite	$MnCO_3$	0.51	0.09
	Rutile	TiO_2	0.16	0.18
	Hydroxilapatite	$Ca_5(PO_4)_3(OH)$	1.13	0.26
	Amorphous		84.7	0.3

3.3. Thermal Analysis Results

The thermal analysis of the five investigated samples showed relevant differences for the weight losses. The results are given in Figure 3.

The first steps in the TGAs, at approximately 100 °C, demonstrated weight losses between 1 and 18 wt%, which were observed in all the samples excluding sample 5. These corresponded to endothermic peaks in the DTA (Figure 4) and can be associated with the loss of hygroscopic water, absorbed after the combustion of oxides [26]. In sample 1, at approximately 400 °C, there was a weight loss of about 50 wt%, corresponding to an exothermic peak in the DTA spectra and associated with the combustion of residual organic matter.

The step at approximately 600 °C could have been related either to the well-known carbonate decomposition reaction ($CaCO_3$ to CaO + CO_2) or to the decomposition of calcium-phosphates ($Ca_3(PO_4)_2$ = CaO + P_2O_5 or K_3PO_4 = $3K_2O$ + P_2O_5) where the phosphorous pentoxide is lost as gas.

On the whole, the total mass losses between 20 and 1200 C varied from 13.38 in sample 2 to 70.84 in sample 1.

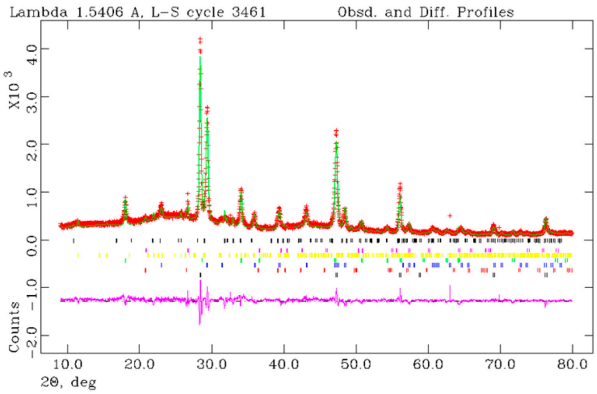

(**a**)

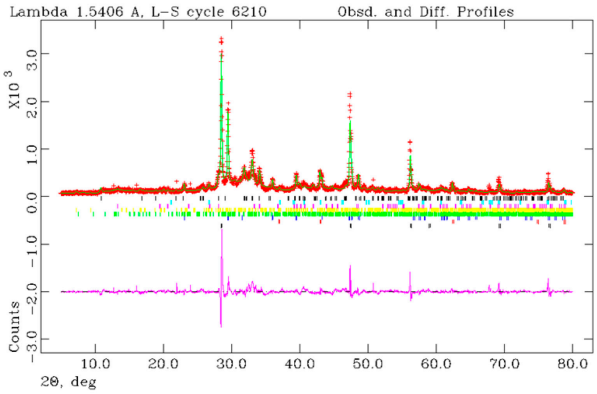

(**b**)

Figure 2. *Cont.*

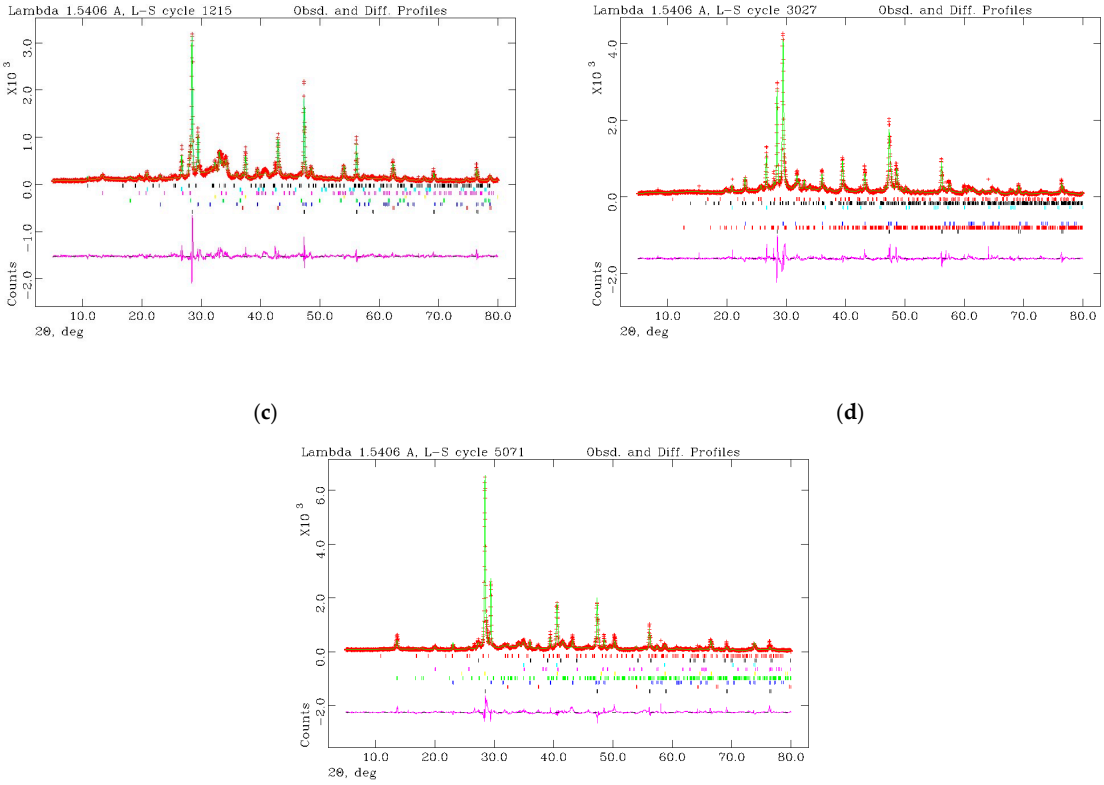

Figure 2. XRPD patterns refined by means of the Rietveld method for samples 1 (**a**), 2 (**b**), 3 (**c**), 4 (**d**), and 5 (**e**). Observed and calculated profiles are given in red and green, respectively. The differences between the observed and calculated powder diffraction profiles are in purple. Thick marks below the diffractograms are the diffraction peak positions per each phase.

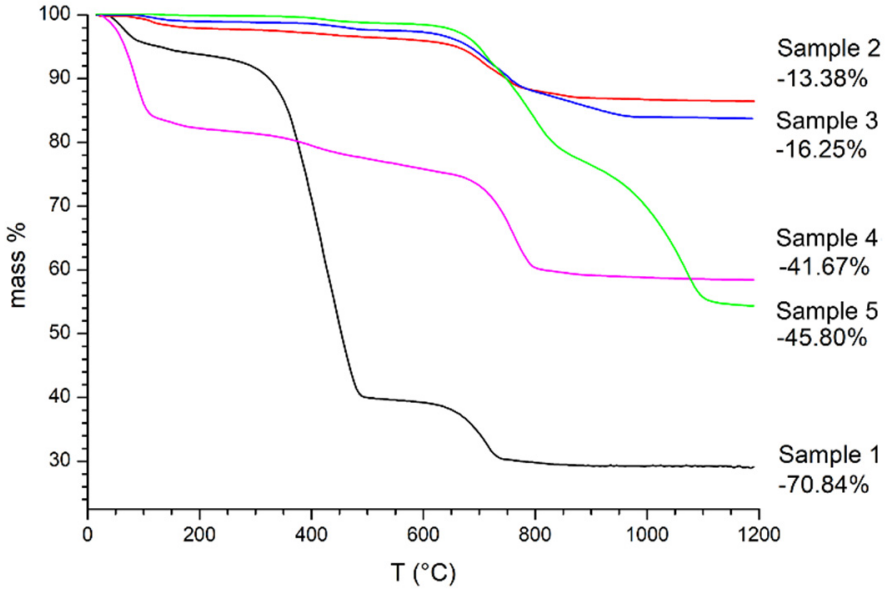

Figure 3. Thermal gravimetric analyses (TGAs) for the five samples of the biomass fly ashes studied.

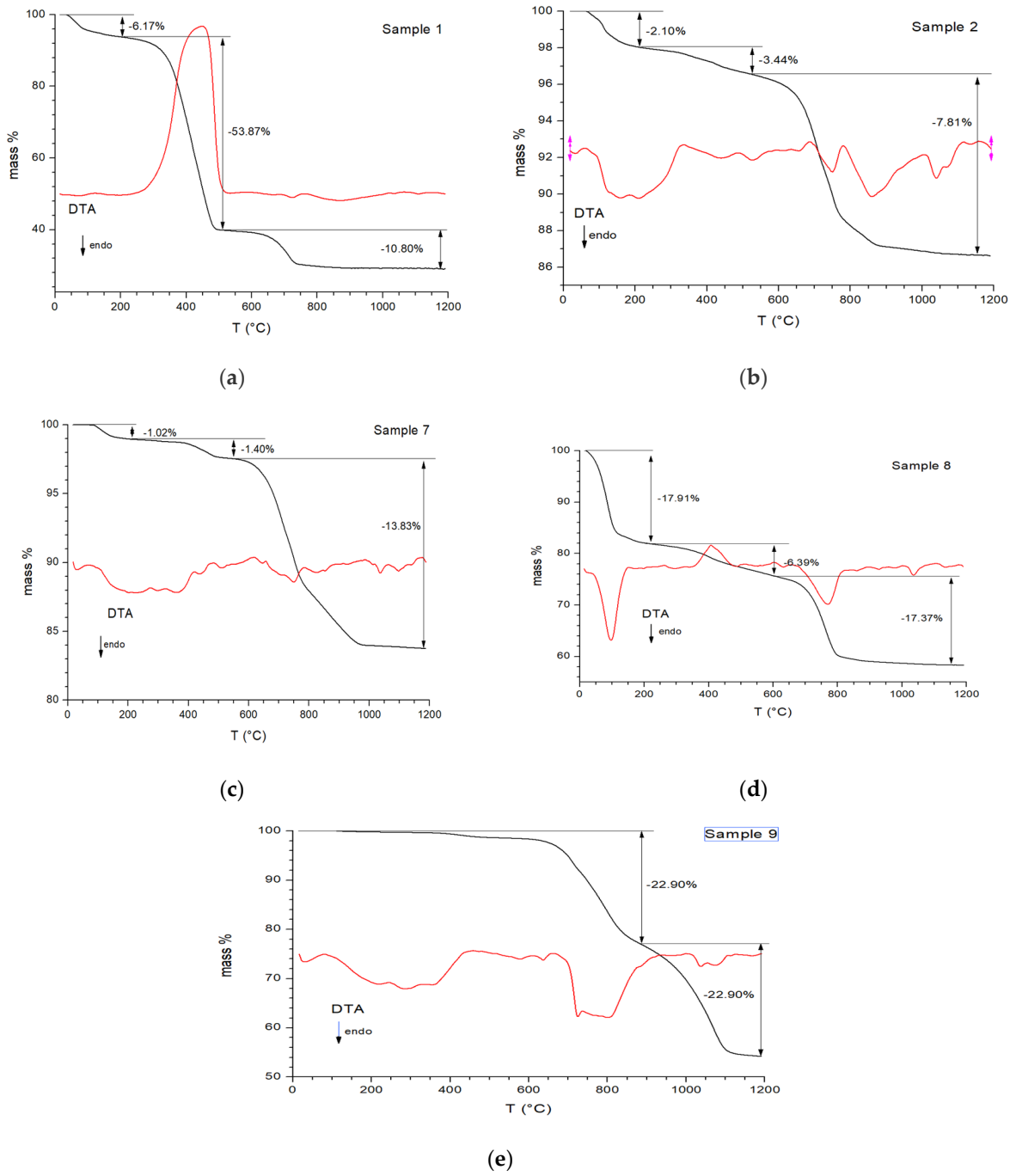

Figure 4. Thermal gravimetric analyses in black and differential thermal analysis (DTA) in red for the five analyzed fly ashes: 1 (**a**), 2 (**b**), 3 (**c**), 4 (**d**), and 5 (**e**).

3.4. Electron Microscopy Results

The results of the FE-SEM analysis coupled with EDS semi-quantitative chemical analysis are shown in Figures 5–8, with interesting textural features shown together with some of the accessory minerals also found by XRPD analysis. Apatite crystals appeared as roundly shaped at sub-micrometric to deci-micrometric sizes (apatite in samples 2 and 5, Figures 5 and 7). Moreover, elongated K_2O and KCl crystals are shown in samples 4 and 5 (Figures 6 and 7).

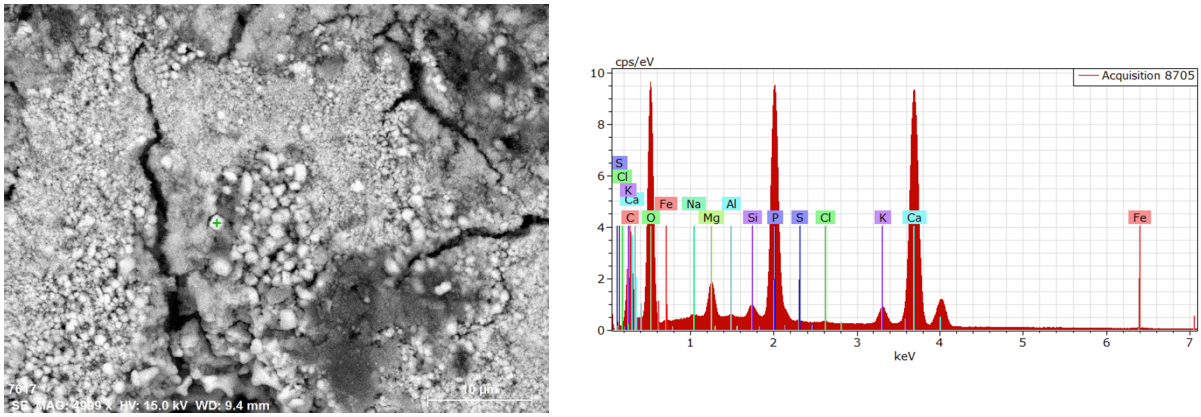

(**a**) (**b**)

Figure 5. FE-SEM analysis of sample 2. On the left (**a**), a secondary electron (SE) image where micrometric sub-spherical crystals of apatite are shown. On the right (**b**), the graph shows the EDS data collected for the apatite crystal at the point indicated with the green cross.

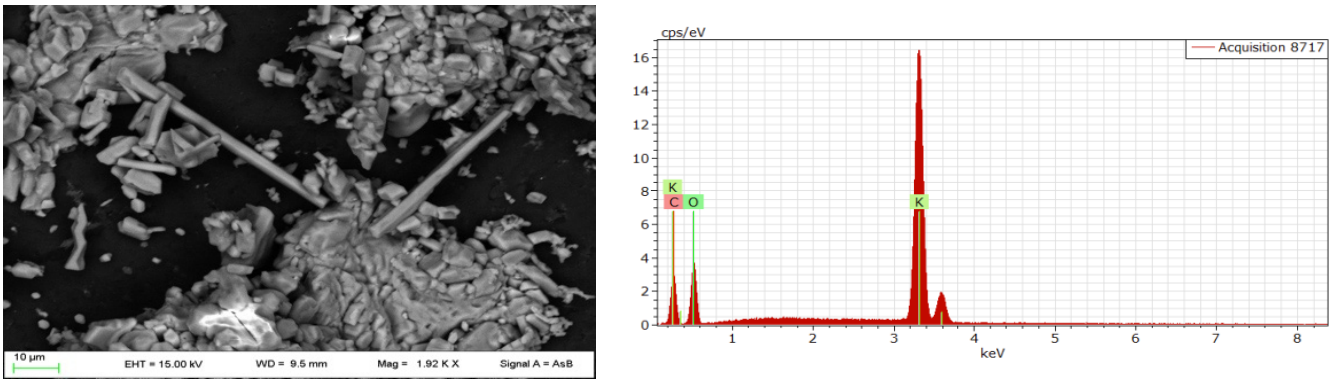

(**a**) (**b**)

Figure 6. FE-SEM analysis of sample 4. On the left (**a**), an SE image with elongated K_2O crystals. On the right (**b**), the EDS data collected for one of the elongated crystals are shown.

Interesting de-vitrification microstructures were also observed in sample 3 (Figure 8). In particular, windmill structures and neoblasts surrounded by glass are shown.

3.5. Chemical Composition Results

The chemical analysis of the major elements in the studied fly ashes (Table 3) indicated that the main component for all of them was CaO, followed by SiO_2 and then Al_2O_3 or, in one case, by MgO. The component P_2O_5 was dominant for sample 2, reaching approximately 9 wt%, whereas for sample 4 the concentration of K_2O reached 5 wt%.

These data fit well with the FE-SEM-EDS microanalysis, where several apatite micro-crystals were found in sample 2 (Figure 5) and an elongated crystal of K_2O in sample 4 (Figure 6).

Potentially toxic elements (PTEs), namely As, Cd, Cr, Cu, F, Pb, Hg, Mo, Ni, Se, V, and Zn, are naturally present in the environment [27] and some of them, in low percentages, can be essential for the correct metabolism of biologic activity. However, when their concentrations increase, they can become toxic. Their accumulation can be caused by anthropogenic activities, such as mining and industrial and agricultural activities [28], and is dependent on their mobility. For most of the PTEs, the mobility increases with the decrease in pH, very rapidly at a pH lesser than 7, whereas at higher pH conditions it slows down. Beyond the pH, other soil parameters, including the organic matter (OM), redox considerations, the chemistry of soil particles, and the composition of clay, affect

the distribution, concentration, and mobility of PTEs. They are considered as hazardous contaminants due to their ability to intoxicate and become aggregated and persistent in the environmental media. For these reasons, several legislative decrees define the concentration limits for PTEs in urban and industrial areas.

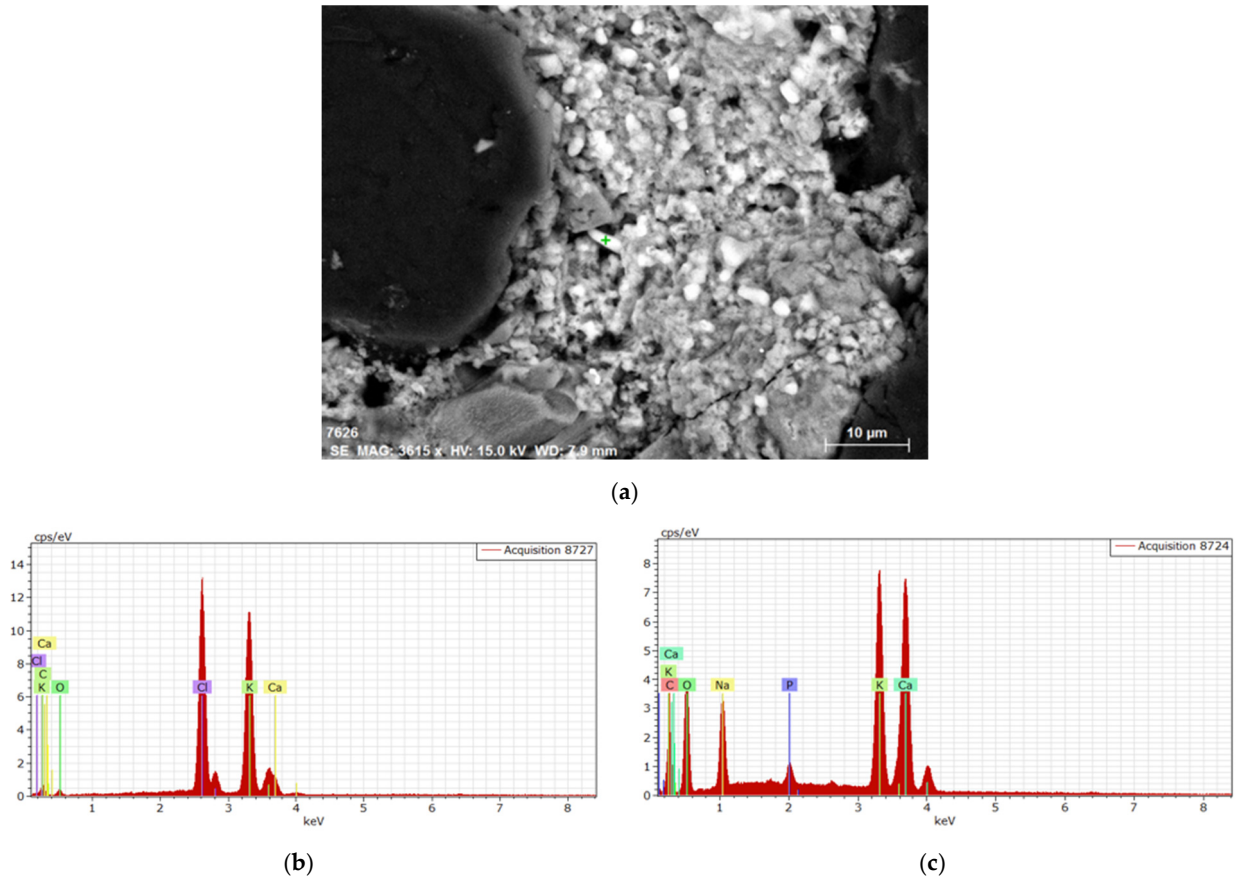

Figure 7. FE-SEM analysis of sample 5. On the left (**a**), an SE image in which elongated and rounded crystals are shown. Below (**b**,**c**), the graphs report the EDS spectra collected for one of the elongated crystals (sylvite, KCl) and for the rounded crystals (apatite, $Ca_5(PO_4)_3(F, OH, Cl)$ crystals), respectively.

Table 3. Major elements (in oxide wt%) measured with EMPA in the five samples.

Sample	#1	#2	#3	#4	#5
NaO	0.08	0.94	0.112	0.582	0.907
Cl	0.30	0.009	0.008	0.006	0.008
MnO	0.146	0.127	1.113	0.121	0.025
K_2O	0.184	1.78	0.005	4.944	0.008
MgO	0.213	9.143	32.39	3.854	1.563
SiO_2	11.76	26.19	16.512	27.949	9.567
Cr_2O_3	0.136	0.0186	0.007	0.014	0.007
FeO	0.611	2.34	2.765	2.889	0.537
CaO	39.84	44.26	37.215	43.31	65.042
Al_2O_3	0.55	5.52	5.540	7.907	1.103
P_2O_5	0.392	8.856	3.508	7.832	7.677
TiO_2	0.067	0.318	0.202	0.349	0.084
Total	54.28	99.515	99.375	99.760	86.53

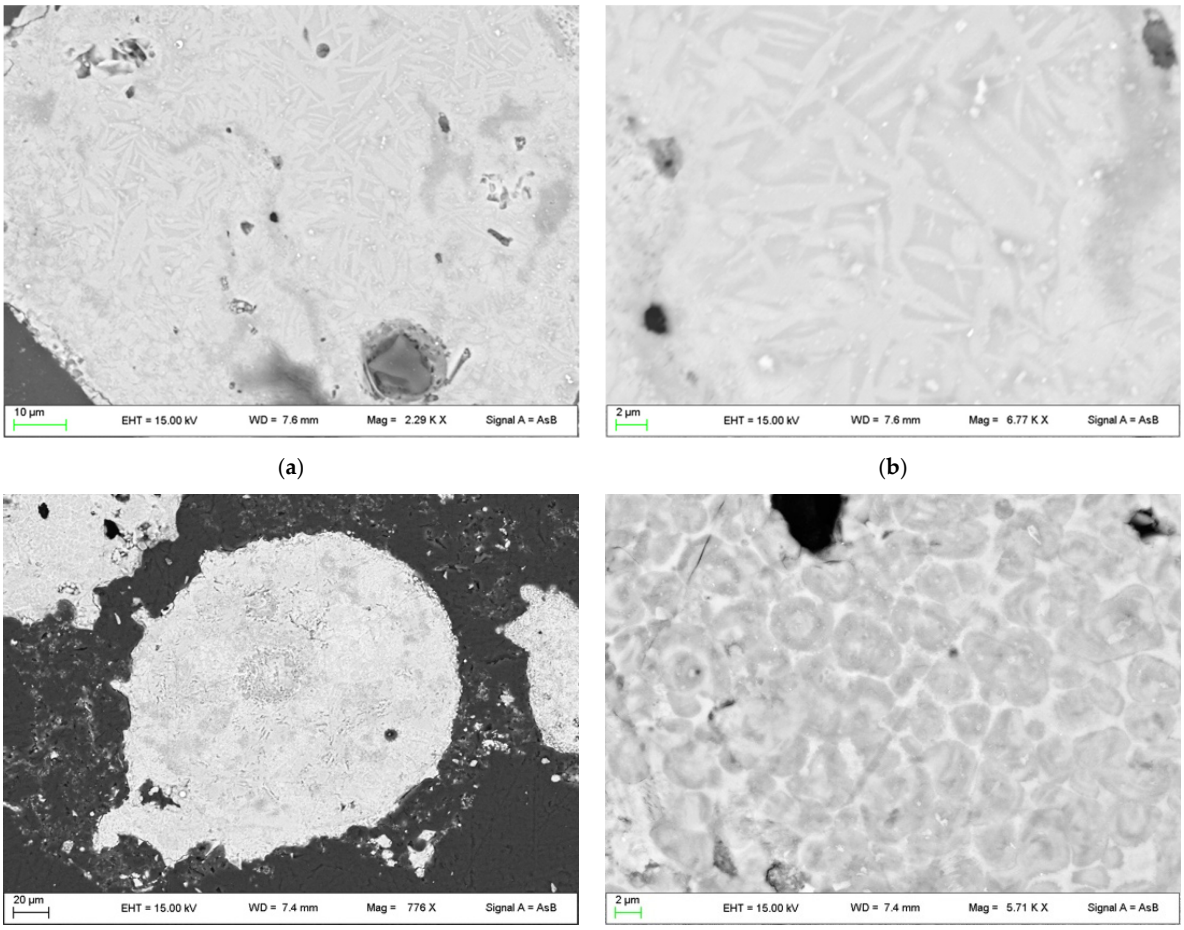

(**a**) (**b**)

(**c**) (**d**)

Figure 8. De-vetrification microstructures observed in sample 3. Above (**a**,**b**), two different magnifications of windmill structures are shown; below (**c**,**d**), two different SE imagines at different magnifications of microstructures showing neoblasts surrounded by glass.

Chemical analyses of PTEs are listed in Table 4 for samples 2, 3, 4, and 5. It was impossible to homogenize sample 1 as it burned during annealing even before melting. In Figure 9, the values of some selected PTEs (V, Cr, Co, Ni, Zn, Pb, Cu, As, Hg, and Se), together with Cl and S, are reported, as measured in the four analyzed samples of fly ashes.

Table 4. Minor elements (ppm) measured with LA-ICP-MS in the four samples (2, 3, 4, and 5).

Sample	#2	#3	#4	#5
V	33.44	32.07	54.08	7.08
Cr	0.13	43.44	0.13	13.55
Co	8.38	22.92	8.44	3.09
Ni	59.40	191.00	51.30	22.18
Zn	479.20	85.20	114.96	51.30
Pb	0.22	0.53	0.13	0.52
Cu	304.62	17.36	153.38	7.85
As	0.25	3.05	0.51	2.21
Cd	0.05	0.23	0.02	0.71
Hg	0.00	0.00	0.00	0.00
Se	0.00	0.00	0.00	0.32
Mo	0.59	184.37	0.23	37.28
Cl	117.40	159.33	97.20	147.80
S	498.63	573.00	314.50	382.00

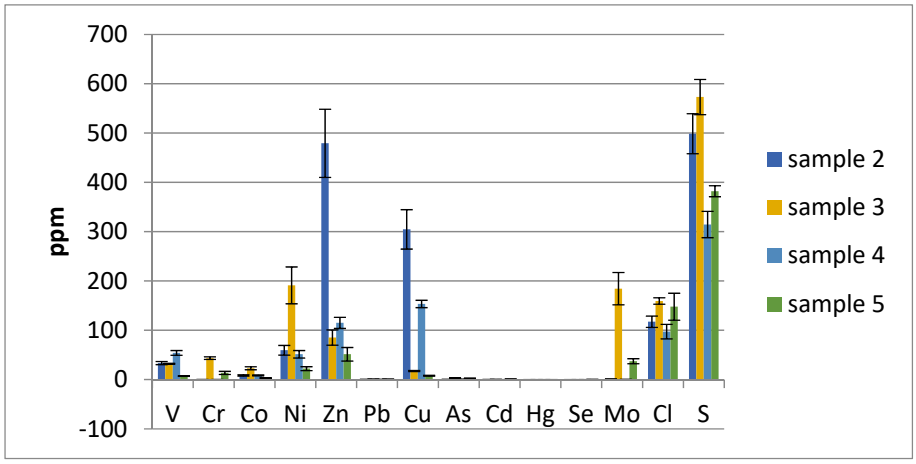

Figure 9. Selected PTE concentrations (V, Cr, Co, Ni, Zn, Pb, Cu, As, Hg, and Se), along with Cl and S concentrations, in the four samples with potentially toxic elements.

The ratios of the measured concentrations of PTEs and the limit concentrations of these same metals for urban and industrial sites, following the Italian legislation (legislative decree 52/2006 Tables 1 and 5, part V), are shown in Figures 10 and 11, respectively.

Table 5. PAH contents in the five samples investigated in the present work. Data are given in mg/kg t.q.

PAH Type/Samples	1	2	3	4	5
Total IPA	1088	<0.050	<0.050	<0.050	<0.050
Naftalene	3706	<0.010	<0.010	<0.010	<0.010
Acenaftene	4.6	<0.010	<0.010	<0.010	<0.010
Acenaftilene	341	<0.010	<0.010	<0.010	<0.010
Fluorene	<0.010	<0.010	<0.010	<0.010	<0.010
Fenantrene	29	<0.010	<0.010	<0.010	<0.010
Antracene	4.0	<0.010	<0.010	<0.010	<0.010
Fluorantene	1.6	<0.010	<0.010	<0.010	<0.010
Pirene	1.3	<0.010	<0.010	<0.010	<0.010
Benzo(a)antracene	0.015	<0.010	<0.010	<0.010	<0.010
Crysene	0.020	<0.010	<0.010	<0.010	<0.010
Benzo(b,k,j)fluorantene	<0.010	<0.010	<0.010	<0.010	<0.010
Benzo(e)pirene	<0.010	<0.010	<0.010	<0.010	<0.010
Benzo(a)pirene	<0.010	<0.010	<0.010	<0.010	<0.010
Indenopirene	<0.010	<0.010	<0.010	<0.010	<0.010
Dibenzo(a,h)antracene	<0.010	<0.010	<0.010	<0.010	<0.010
Benzo(g,h,i)perilene	<0.010	<0.010	<0.010	<0.010	<0.010

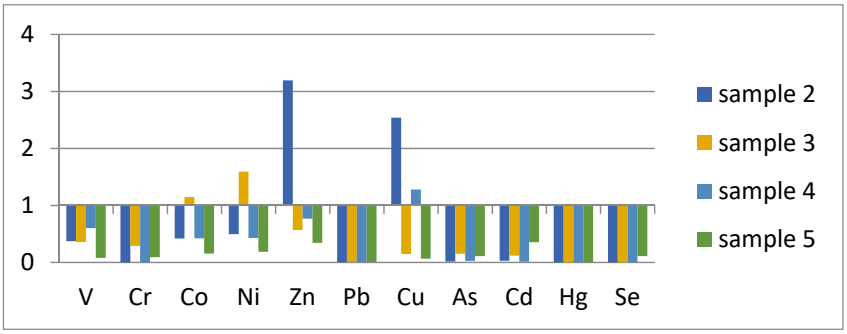

Figure 10. Ratios between the measured concentrations of V, Cr, Co, Ni, Zn, Pb, Cu, As, Hg, and Se in the four samples (Figure 9) and the values for the Italian limits of those metals for urban sites.

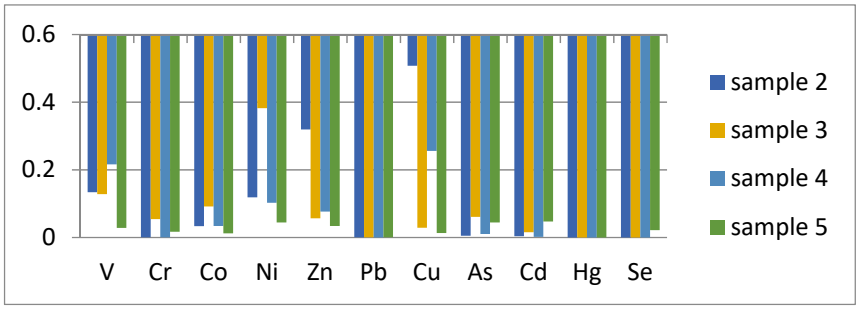

Figure 11. Ratios between the measured concentrations of V, Cr, Co, Ni, Zn, Pb, Cu, As, Hg, and Se in the four samples (Figure 9) and the values for the Italian limits of those metals for industrial sites.

All samples had PTE concentrations below the legislative limit for industrial sites and only sample 2 had Cu and Zn, and sample 4 Cu, with values above the legislative limits.

The total amount of the PAHs naftalene, acenaftene, acenaftilene, fluorene, fenatrene, antracene, fluoratene, pirene, benzoantracene crysene, benzo(b,k,j) fluorantene, benzo(e)pirene, benzo(a)pirene, indenopirene, dibenzo(a,h)antracene, and benzo(g,h,i)perilene (Table 5) were below the detection limits for all the investigated samples, with the exception of sample 1, which came from a gasification plant.

4. Discussion

The comparison of the multi-methodological analyses performed here on five samples coming from fly ashes of different vegetal biomasses allows us to outline the following considerations:

1. The PTE concentrations were evaluated for the potential human and ecological risks, since their accumulation increases the toxic hazard [29,30]. In all of the samples of fly ashes from biomasses, the PTE concentrations analyzed were below the limits indicated in Italian legislation. Moreover, the PAH content was undetectable for all samples with the exception of sample 1, which was a unique sample coming from a gasification plant.
2. Gasification is a process that converts either biomass [31] or fossil fuel-based carbonaceous materials into gases. The process consists of the reaction of the feedstock material, at high temperatures (typically > 700 °C) without combustion, via control of the amount of oxygen and/or steam present in the reaction. The resulting gas mixture is called syngas (from synthesis gas) or producer gas and its largest fraction is composed of nitrogen (N_2), carbon monoxide (CO), hydrogen (H_2), and carbon dioxide (CO_2). Due to the flammability properties of the H_2 and CO, syngas is itself a fuel. The thermal analysis performed in this work showed a strong weight loss, more than 50 wt%, at approximately 400 °C for sample 1. Indeed, during the process some material remained un-combusted, likely due to the large amount of PAH content in that sample.
3. The granulometric analysis indicated that the PM2.5 fraction, namely the amount of particles with average dimensions below 2.5 μm, which can represent a danger to human health due to their potential of being inhaled, was significantly lower than 1%; the amount of particles with diameters less than 10 μm was quite different, varying from 5% in sample 5 to 40% in sample 4.
4. The high phosphorous content, as an apatite mineral, as well potassium content, as a sylvite mineral, suggests that these materials may represent good amendments for agricultural lands once the bioavailability of these elements is proved and verified. The electron microscopy analysis showed that the crystals usually have very small dimensions, from the nanometer scale to a few microns. Moreover, the Rietveld analysis indicated that the amorphous content in all samples was very high, ranging from 47.6 wt% in sample 1 up to 84.7 wt% in sample 5. Both the above-mentioned

characteristics are good indicators of a large reaction surface, one the most important parameters for bioavailability.

5. The high Ca content revealed by the chemical analysis did not have a counterpart in the mineralogical composition of the samples, as relevant amounts of Ca minerals were not observed in the XRPD data processing. Thus, the high Ca content is supposedly stored in the amorphous phase, which was quite abundant in the studied fly ashes.
6. The high Ca content measured in the samples suggests that these materials can be used as amendments in soils, usually clayey soils, with low geotechnical properties. In these soils, the traditional addition of CaO, coming from the decarbonation reaction of carbonate minerals, improves the mechanical properties as pozzolanic reactions induced by the highly alkaline environment promote the formation of new binding compounds such as calcium silicate hydrate minerals (C-A-H; C-S-H) [32–34]. In a high pH environment, natural pozzolanas, rich in silicon and amorphous phase, promote pozzolanic reactions as they increase the availability of silicon and alumina [35]. The large amount of amorphous content, evidenced by the Rietveld analysis, and the chemical compositions of the analyzed ash samples suggest that at least some of them could be successfully used in combination with or as substitutions for traditional binders in soil stabilization. Such use would require the environment to reach the alkalinity needed to promote pozzolanic reactions, with or without the addition of alkaline activators, which are normally used for soil treatment by means of fly ashes [35].

5. Conclusions

The addition of Ca from fly ashes in soil with poor geotechnical properties may represent a good example of end of waste. In fact, in this way, two waste materials, namely fly ashes and clayey soils, can be reconverted into a good second-generation product, thus avoiding the removal and transport of the soils and the opening of new caves for the extraction of carbonate, as well as reducing the CO_2 emissions from transports and de-carbonatation reactions.

The present study indicates that the dimensions and the chemical compositions of the studied fly ashes, namely the low concentrations of PTEs and PAHs (with the exception of the sample from the gasification plant), as well as the high CaO content in the amorphous fraction, represent favorable factors that can enhance interest in the applicability areas of these products. In fact, biomass fly ashes could be used as amendments in clayey soils to substitute for lime and stimulate pozzolanic reactions and improve their geotechnical properties. Further experiments to check the effect of the addition of fly ashes with high CaO content in clayey soils are in progress.

Moreover, the application of P fertilizer in intensive crop and animal production systems has increased pressure on finite global reserves of phosphate rocks [36], and their availability worldwide has recently drawn important criticisms due to both the high depletion of natural reserves and their geo-localization in limited areas.

Biomass fly ashes demonstrate high levels of phosphorous and potassium contents, which are present in nano/micro-crystals (as shown by electron microscopy) that biomasses have assimilated during their life cycle. The possibility that biomass fly ashes could be used as agricultural fertilizes opens an interesting perspective on a new and ecological source of K and P.

The above-mentioned scenarios fit well with the principles of the circular economy, in which waste materials, such as biomass fly ashes, could be recycled and used as second-generation products, thus avoiding the need to mine natural raw materials, such as carbonated and phosphate rocks.

Author Contributions: Conceptualization, P.C., F.C. and G.C.; methodology, P.C., A.Z., U.S., G.C., R.V. and C.C.; validation, A.Z., U.S. and P.C.; resources, P.C.; data curation, P.C., A.Z., U.S., G.C., R.V, P.C., A.Z. and C.C.; funding acquisition, P.C. All authors have read and agreed to the published version of the manuscript.

Funding: This research was founded by the Fondazione Cassa di Risparmio di Perugia (Italy) with the title: Ceneri da biomassa e da carbone: possibili reimpieghi e strategie di bonifica. Project number: #2018.0508.

Institutional Review Board Statement: Not applicable.

Informed Consent Statement: Not applicable.

Data Availability Statement: The data presented in this study are available on request from the corresponding author.

Conflicts of Interest: The authors declare no conflict of interest.

References

1. Torquati, B.; Marino, D.; Venanzi, S.; Porceddu, P.; Chiorri, M. Using tree crop pruning residues for energy purposes: A spatial analysis and an evaluation of the economic and environmental sustainability. *Biomass Bioenergy* **2016**, *95*, 124–131. [CrossRef]
2. James, A.K.; Thring, R.W.; Helle, S.; Ghuman, H.S. Ash Management Review—Applications of Biomass Bottom Ash. *Energies* **2012**, *5*, 3856–3873. [CrossRef]
3. Cavalaglio, G.; Cotana, F.; Nicolini, A.; Coccia, V.; Petrozzi, A.; Formica, A.; Bertini, A. Characterization of Various Biomass Feedstock Suitable for Small-Scale Energy Plants as Preliminary Activity of Biocheaper Project. *Sustainibility* **2020**, *12*, 6678. [CrossRef]
4. Michalik, M.; Wilczynska-Michalik, W. Mineral and chemical composition of biomass ash. In Proceedings of the European Mineralogical Conference, Frankfurt, Germany, 2–6 September 2012; Volume 1.
5. Kalembkiewicz, J.; Galas, D.; Sitarz-Palczak, E. The Physicochemical Properties and Composition of Biomass Ash and Evaluating Directions of its Applications. *Pol. J. Environ. Stud.* **2018**, *27*, 2593–2603. [CrossRef]
6. Zając, G.; Szyszlak-Bargłowicz, J.; Gołębiowski, W.; Szczepanik, M. Chemical Characteristics of Biomass Ashes. *Energies* **2018**, *11*, 2885. [CrossRef]
7. Obenberger, L.; Supancic, K. Possibilities of ash utilization from biomass combustion plants. In Proceedings of the 17th European Biomass Conference and Exhibition, Hamburg, Germany, 29 June–3 July 2009.
8. Carević, I.; Štirmer, N.; Trkmić, M.; Kostanić Jurić, K. Leaching Characteristics of Wood Biomass Fly Ash Cement Composites. *Appl. Sci.* **2020**, *10*, 8704. [CrossRef]
9. Wang, S.; Baxter, L. Comprehensive study of biomass fly ash in concrete: Strength, microscopy, kinetics and durability. *Fuel Process. Technol.* **2007**, *88*, 1165–1170. [CrossRef]
10. Salvo, M.; Rizzo, S.; Caldirola, M.; Novajra, G.; Canonico, F.; Bianchi, M.; Ferraris, M. Biomass ash as supplementary cementitious material (SCM). *Adv. Appl. Ceram.* **2015**, *114*, S3–S10. [CrossRef]
11. Cabrera, M.; Díaz-López, J.L.; Agrela, F.; Rosales, J. Eco-Efficient Cement-Based Materials Using Biomass Bottom Ash: A Review. *Appl. Sci.* **2020**, *10*, 8026. [CrossRef]
12. Rajamma, R.; Ball, R.J.; Tarelho, L.A.C.; Allen, G.C.; Labrincha, J.A.; Ferreira, V.M. Characterization and use of bio-mass fly ash in cement-based materials. *J. Hazard. Mater.* **2009**, *172*, 1049–1060. [CrossRef]
13. Sun, L.; Gong, K. Silicon-Based Materials from Rice Husks and Their Applications. *Ind. Eng. Chem. Res.* **2001**, *40*, 5861–5877. [CrossRef]
14. Soltani, N.; Bahrami, A.; Pech-Canul, M.I.; González, L.A. Review on the physicochemical treatments of rice husk for production of advanced materials. *Chem. Eng. J.* **2015**, *264*, 899–935. [CrossRef]
15. Demirbaş, A. Heavy metal contents of fly ashes from selected biomass samples. *Energy Sources* **2005**, *27*, 1269–1276. [CrossRef]
16. Boström, C.E.; Gerde, P.; Hanberg, A.; Jemstrom, B.; Johansson, C.; Kyrkslund, T.; Ranung, A.; Tomqvist, M.; Victorin, K.; Westerholm, R. Cancer risk assessment, indicators, and guidelines for polycyclic aromatic hydrocar-bons in the ambient. *Environ. Health Perspect.* **2002**, *110*, 451–488. [PubMed]
17. Baird, W.M.; Hooven, L.A.; Mahdevan, B. Carcinogenic polycyclic aromatic hydrocarbon-DNA adducts and mechanism of action. *Environ. Mol. Mutagen.* **2005**, *2–3*, 106–114. [CrossRef]
18. Haykırı-Açma, H. Combustion characteristics of different biomass materials. *Energy Convers. Manag.* **2003**, *44*, 155–162. [CrossRef]
19. Cai, J.; He, Y.; Yu, X.; Banks, S.W.; Yang, Y.; Zhang, X.; Yu, Y.; Liu, R.; Bridgwater, A.V. Review of physicochemical properties and analytical characterization of lignocellulosic biomass. *Renew. Sustain. Energy Rev.* **2017**, *76*, 309–322. [CrossRef]
20. Hasler, P.; Nussbaumer, T. Particle size distribution of the fly ash from biomass combustion. In Proceedings of the 10th European Conference and Technology Exhibition Biomass for Energy and Industry, Wurzburg, Germany, 8–11 June 1998.
21. Rietveld, H.M. A profile refinement method for nuclear and magnetic structures. *J. Appl. Cryst.* **1969**, *2*, 65–71. [CrossRef]

22. Larson, A.C.; Von Dreele, R.B. *Generalized Structure Analysis System (GSAS) LANSCE, MS-H805*; Los Alamos National Laboratory: Los Alamos, NM, USA, 2000; p. 87545.
23. Toby, B.H. EXPGUI, a graphical user interface for GSAS. *J. Appl. Crystallogr.* **2001**, *34*, 210–213. [CrossRef]
24. Gentili, S.; Comodi, P.; Nazzareni, S.; Zucchini, A. The orvieto-Bagnoregio ignimbrite: Pyroxene crystalchemistry and bulk pahse composition of pyroclastic deposits, a tool to identify sym and post-depositional processes. *Eur. J. Mineral.* **2014**, *26*, 743–756. [CrossRef]
25. Petrelli, M.; Morgavi, D.; Vetere, F.; Perugini, D. Elemental Imaging and Petro-Volcanological Applications of an Improved Laser Ablation Inductively Coupled Quadrupole Plasma Mass Spectrometry. *Period. Mineral.* **2016**. [CrossRef]
26. Balic-Zunic, T.; Birkedal, R.; Katerinopoulou, A.; Comodi, P. Dehydration of bloedite, $Na_2Mg(SO_4)_2(H_2O)_4$ and leonite $K_2Mg(SO_4)_2(H_2O)_4$. *Eur. J. Mineral.* **2016**, *28*, 33–42. [CrossRef]
27. Frondini, F.; Zucchini, A.; Comodi, P. Water-rock interaction and trace elements distribution in dolomite aquifers: The Sassolungo and Sella system (Northern Italy). *Geochem. J.* **2014**, *48*, 231–246. [CrossRef]
28. Saddique, U.; Muhammad, S.; Tariq, M.; Zhang, H.; Arif, M.; Isthtiaq, A.K.; Khattak, N.U. Potentially toxic elements in soil of the Khyber Pakhtunkhwa province and Tribal areas, Pakistan: Evaluation for human and ecological risk. *Environ. Geochem. Health* **2018**, *40*, 2177–2190. [CrossRef]
29. Palansooriya, K.N.; Shaheen, M.S.; Chen, S.S.; Tsang, D.C.W.; Hashimoto, Y.; Hou, D.; Bolan, N.S.; Rinklebe, J.; Ok, Y.S. Soil amendments for immobilization of potentially toxic elements in contaminated soils: A critical review. *Environ. Int.* **2020**, *134*, 105046. [CrossRef]
30. Ur Rehman, I.; Ishaq, M.; Ali, L.; Muhammad, S.; Ud Din, I.; Yaseen, M.; Ullah, H. Potentially toxic elements' occurrence and risk assessment through water and soil of Chitral urban environment, Pakistan: A case study. *Environ. Geochem. Health* **2020**, *42*, 4355–4368. [CrossRef] [PubMed]
31. Schulzke, T. Biomass gasification: Conversion of forest residues into heat, electricity and base chemicals. *Chem. Pap.* **2019**, *73*, 1833–1852. [CrossRef]
32. Bell, F.G. Lime stabilization of clay minerals and soils. *Eng. Geol.* **1996**, *42*, 223–237. [CrossRef]
33. Al-Mukhtar, M.; Lasledj, A.; Alcover, J.F. Behaviour and mineralogy changes in lime-treated expansive soil at 20 °C. *Appl. Clay Sci.* **2010**, *50*, 191–198. [CrossRef]
34. Guidobaldi, G.; Cambi, C.; Cecconi, M.; Comodi, P.; Deneele, D.; Paris, M.; Russo, G.; Vitale, E.; Zucchini, A. Chemo-Mineralogical evolution and microstructural modifications of a lime treated pyroclastic soil. *Eng. Geol.* **2018**, *245*, 333–343. [CrossRef]
35. Vitale, E.; Russo, G.; Dell'Agli, G.; Ferone, C.; Bartolomeo, C. Mechanical behaviour of soil improved by alkali activated binders. *Environments* **2017**, *4*, 80. [CrossRef]
36. Rowe, E.; Withers, A.J.; Baas, P.; Chan, N.; Doody, D.; Holiman, J.; Jacobs, B.; Li, H.; MacDonald, G.K.; McDowell, R.; et al. Integrating legacy soil phosphorus into sustainable nutrient management strategies for future food, bioenergy and water security. *Nutr. Cycling Agroecosyst.* **2016**, *104*, 393–412. [CrossRef]